**ORIGINAL PAPER**

# Simulation of a heavy rainfall event during southwest monsoon using high-resolution NCUM-modeling system: a case study

Devajyoti Dutta[1] · A. Routray[1] · D. Preveen Kumar[1] · John P. George[1] · Vivek Singh[1]

## Abstract

The study is undertaken to demonstrate and evaluate the skill of National Centre for Medium Range Weather and Forecasting (NCMRWF) Unified Model (NCUM) model with different horizontal resolutions in simulation of a heavy rainfall event (26–29 July 2015) occurred over Gujarat and Rajasthan region due to the presence of monsoon depression (MD). For this purpose, three numerical experiments are carried out such as NCUM12, NCUM4, and NCUM1.5 by configuring the NCUM model with different horizontal resolutions 12, 4 and 1.5 km, respectively. In all the experiments, the model is integrated for 72 h from 00 UTC of 26 July 2015. The model integration time step is considered for NCUM12 (300 s), NCUM4 (60 s), and NCUM1.5 (60 s). The overall results suggested that the high-resolution NCUM1.5 is reasonably well-simulated the position, northeastward movement as well as the pattern and intensity of rainfall associated with the MD as compared to the NCUM12 and NCUM4 simulations. The mean Direct Position Errors (DPEs) are reduced by 7 and 22% in the NCUM1.5 over NCUM4 and NCUM12 simulations. The intensity forecast based on 10 m maximum sustainable wind (MSW) is reasonably well-simulated in the NCUM1.5 as compared to other simulations. The mean percentage of error of MSW is about 39, 30, and 26% in the NCUM12, NCUM4, and NCUM1.5 simulations, respectively. It is showing that the intensity of the MD is realistically simulated in the high-resolution NCUM model. The CAPE value is improved by 47, 59, and 68%, in the NCUM12, NCUM4, and NCUM1.5, respectively. The skew-T plot suggested that the convection is more prominent in the NCUM1.5 simulation, which is reasonably well matched with the observation. The mean skill of HSS score from NCUM1.5 is improved by 67% (73%) and 40% (28%) with respect to the NCUM12 and NCUM4 simulations during day 1 (day 2), respectively. Further verification of this rainfall event is carried out based on the contiguous rain area (CRA) technique. The total mean square error (MSE) in day 1 is reduced by 35 and 16% in the NCUM1.5 simulation with respect to NCUM12 and NCUM4 for 5 cm threshold, respectively. Similarly, for 10 cm threshold, MSE in NCUM1.5 simulation is reduced by 16 and 14% with respect to NCUM12 and NCUM4 simulation, respectively. This verification technique also confirms that the better skill of NCUM1.5 over other simulations in terms of pattern, location, and volume errors of the rainfall with different thresholds.

## 1 Introduction

The heavy to extreme rainfall events [defined by Indian Meteorological Department (IMD) as heavy rainfall 64.5–124.4 mm; very heavy rainfall 124.5–244.4 mm and extremely heavy rainfall more than or equal to 244.5 mm per day] are regularly experienced by Indian sub-continent

mainly along the west coast during the summer monsoon (June–September). These rainfall events contribute significantly to the all India rainfall during the south-west monsoon (SWM). The heavy rainfall events along the west coast of India and other parts of the country occur due to the presence of organized meso-convective systems (MCSs), which are embedded in large-scale monsoonal circulations like off-shore troughs and vortices, depressions over the Bay of Bengal (BoB)/Arabian Sea, and mid-tropospheric cyclones (Sikka and Gadgil 1980; Benson and Rao 1987; Zipser et al. 2006). The extreme rainfall events have significant impact on the society, economy, and environment by causing flash floods, landslides, etc. Therefore, timely and accurately prediction of such rainfall events is highly desirable for disaster

warnings and mitigation efforts and thereby minimizing human casualties and property damage considerably.

Forecasting heavy rainfall is especially difficult, since it involves complex interaction with the surrounding environment and the resultant of heavy rainfall event impacts on quantitative precipitation forecast (QPF), which is recognized as a challenging task (Charles 1993). In the last two decades, the numerical models have evolved to predict the extreme weathers, which lead to heavy rainfall events over Indian monsoon region (Routray et al. 2005, 2010a; Vaidya and Kulkarni 2007; Deb et al. 2008; Kumar et al. 2008; Chang et al. 2009; Mohanty et al. 2012). However, the forecast skill of the models is very limited, particularly for prediction of precipitation (Bhowmik and Prasad 2001; Rama Rao et al. 2007; Sikka and Rao 2008; Das et al. 2008; Routray et al. 2010b, 2016). Many approaches are used to improve the forecast skill of numerical models viz. improvement of physical parameterization schemes and improve the model initial condition through advance data assimilation techniques, increased model resolution, multi- model ensemble, inclusion of hydrological processes affected by the evapo-transpiration, etc. (Rajeevan et al. 2010; Routray et al. 2010a; Durai et al. 2014; David et al. 2010, etc.).

The model simulations/predictions can be improved by increasing the model resolution, because the high-resolution model can better represent the atmospheric dynamics and mesoscale forcing and assimilate the high-resolution observations through data assimilation (Colle et al. 2000; Kalnay et al. 2003). Many studies show that an increase in the model resolution improves the rainfall forecasts associated with the large-scale circulation, for example, the Mumbai heavy rainfall event (Mohanty et al. 2012), evolution of squall lines (Weisman et al. 1997), extreme rainfall events (Nielson and Strack 2000; Deb et al. 2008; Kumar et al. 2008; Lee et al. 2011), and mesoscale convective evolutions (Bernadet et al. 2000; Chien et al. 2001). Wang and Seaman (1997); Lee et al. (2011) and Hong (2004) studied the effects of different horizontal resolutions on simulating precipitation in numerical models. They found that the precipitation intensity and spatial distribution show high sensitivity to horizontal resolution; however, the impacts of physical parameterization schemes also play a significant role on precipitation simulation than changing the resolution. By increasing the model resolution, the topography is better represented, which plays an important role for severe precipitation forecasting (Zhang et al. 2009; Davolio et al. 2009; Heikkilä et al. 2011; Xie and Zhang, 2012, Jung, 2016).

The National Centre for Medium Range Weather and Forecasting (NCMRWF) is running the Unified Model (NCUM) of UK Met Office as operational global model (Davies et al. 2005; Rajagopal et al. 2012) and the global model have yielded mixed results on prediction extreme rainfall events (Dube et al. 2014; Ashrit et al. 2015;

Unnikrishnan et al. 2016). O'Hara and Webster (2012) studied the effects of different horizontal resolutions (1.5 km, 4 km and 24 km) on simulating the hurricane Katrina using UK Met Office Unified Model (UM) and found that the structure and intensity of the hurricane Katrina are more sensitive to the horizontal resolution. Lean et al. (2008) pointed out that the high-resolution UM model is capable to reproduce the convective cells and time of initiations of convection correctly, which lead to the rainfall event. The high-resolution UM model also predicted the severe and hazardous strong wind events associated with the enhancement of katabatic winds by synoptic weather systems over Antarctic coast during the winter (Orr et al. 2014).

There have been not many studies to assess the impact of resolution in the forecasting of heavy rainfall events over Indian monsoon region using NCUM model. The study, therefore, is undertaken to demonstrate and evaluate the skill of NCUM model with different horizontal resolutions (12, 4, and 1.5 km) in the simulation of a heavy rainfall event (27–29 July 2015), which occurred over Gujarat (22.25°N, 71.19°E) and Rajasthan (27.39°N, Lon 73.43°E) region due to the presence of MD during the active phase of SWM. The study is carried out only with the high-resolution models without data assimilation, and the advantage is that properties of the models are not influenced by the effects from the assimilation system. The synoptic condition associated with the heavy rainfall event is presented in Sect. 2. Section 3 illustrates the rainfall event analyzed through satellite data sets and skew-T diagram. Section 4 presents a brief description of the NCUM-modeling system, the numerical experiments and methods, and results and discussion are presented in Sect. 5. Conclusion of the study is presented in Sect. 6.

## 2 Synoptic conditions during 27–29 July 2015

A well-marked low-pressure area was formed over east Rajasthan and neighbourhood on 26th July 2015. On 27th July 2015, the low pressure concentrated into a depression situated over southwest Rajasthan and neighbourhood. It is further intensified into deep depression laid over southwest Rajasthan and adjoining Gujarat at 03 UTC of 28th July 2015 and remained over the same region up to 12 UTC of 28th July 2015. The lowest central pressure around 990 hPa and maximum sustained wind speed of 25 kts observed during 28th July 2015. The system moved north-northeastwards and weakened into a depression over west Rajasthan about 40 km south-southwest of Bikaner at 03 UTC of 29th July 2015. It further moved north-northeastward and weakened into a well-marked low-pressure area over the west Rajasthan and neighbourhood on 30th July 2015. During this period active to vigorous monsoon conditions prevailed over

Rajasthan, Gujarat state and west Madhya Pradesh due to the presence of the deep depression and heavy to extremely heavy rainfall occurred over these regions. Accumulated heavy rainfall more than 260 mm occurred during 5 days led to devastating floods, loss of crops, and human lives in several parts of Gujarat and Rajasthan. The cloud imageries from INSAT-3D infrared channel collected from IMD (Fig. 1a–c) depicted at different stages of the system and the strong convective cloud bands associated with the system are clearly seen over Gujarat and Rajasthan regions.

## 3 Analyzing the rainfall event through satellite and Skew-T diagram

In this section, the rainfall event is analyzing through the available satellite data set mainly from Global Precipitation Mission (GPM) and skew-T diagram. The heavy rainfall, flash floods are increasing due to the global environmental changes, which are now a major concern in worldwide (Goswami et al. 2006; Dash et al. 2009). To study such events, utilizing observation technology for that GPM project (Hou et al. 2014) has been developed under international cooperation. The GPM core satellite has been cooperatively developed by the National Aeronautics and Space Administration (NASA) and Japan Aerospace Exploration Agency (JAXA). The satellite carries a Dual-frequency Precipitation Radar (DPR) and GPM Microwave Imager (GMI) on board (Hamada et al. 2016).

The spatial plot of GPM microwave imagery (GMI) and GPM radar as well as vertical cross section (height and distance) of the GPM radar valid at 27 July 2015 are depicted in Fig. 1d–f, respectively. The spatial plot of GMI (Fig. 1d) and radar (Fig. 1e) is shown strong convective band of clouds over Gujarat region. The GPM radar is captured the small portion of the convective system due to smaller swath during the period. However, the radar reflectivity ranged from 30 to 50 dBz is spreading over maximum regions, and it is suggested that the heavy rainfall was occurred over that region. The vertical cross section of radar (Fig. 1f) showed severe convection and extended up to 17 km as well as covered large areas around 50 km radius. It is clearly seen from the Fig. 1f that the reflectivity (~ 40–50 dBz) vertically extended up to 10 km due to strong convection occurred over the region. Overall, the GPM satellite is able to capture the heavy rainfall events over the region.

Figure 2a–c depicts the Rawinsonde data plotted on a Skew-T (logp) graph (http://weather.uwyo.edu/upperair/sounding.html) from Jodhpur (lat. 26.3°N and lon. 73.01°E), Rajashthan at 00 UTC 27–29 July 2015, respectively. The Skew-T plot (Fig. 2a, b) indicates that the entire atmosphere was highly unstable during 27th and 28th July 2015. The instability of the atmosphere is measured by the separation

of the curve of air parcel lapse rate and environmental lapse rate. It is noticed that the instability of the atmosphere increased gradually from 27th to 28th July 2015 due to the change in the intensity of monsoon depression (depression to deep depression). However, the convective available potential energy (CAPE) is lower ($174$ Jkg$^{-1}$) in 28th July (Fig. 2b) as compared to the CAPE ($225$ Jkg$^{-1}$) in 27th July (Fig. 2c), possibly the CAPE is utilized to intensify the system. The maximum instability of the atmosphere is observed around 300 hPa level in both the days. During these days, the convective inhibition (CIN) remained very low, indicating the favorable conditions for the system. In Fig. 2c, it is seen that the whole atmosphere is stable and the CAPE reduced to a value of $1.07$ Jkg$^{-1}$ due to the weakened the monsoon system.

## 4 Model, numerical experiment, and verification methodology

The NCUM model (Version 8.5) is a non-hydrostatic model with rotated latitude–longitude horizontal grid and Arakawa-C staggering and a terrain-following hybrid-height vertical coordinate with Charney-Philips staggering (Davies et al. 2005). The wind components (u, v, and w), potential temperature, exner pressure, density, and three components of moisture viz. vapour, cloud water, and cloud ice are major model variables. The rotated latitude–longitude grid ensures a quasi-uniform grid length over the whole integration domain. The NCUM model used semi-implicit, semi-Lagrangian, predictor corrector numerical scheme (Cullen et al. 1997; Davies et al. 2005) to solve the deep-atmosphere dynamics. The predictor step includes all the processes (including the physics), but approximates some of the (non-linear) terms. The model includes different types of physical parameterization schemes such as surface (Essery et al. 2001), boundary layer (Lock et al. 2000; Martin et al. 2000), mixed-phase cloud microphysics (Wilson and Ballard 1999), and convection (Gregory and Rowntree 1990; Grant and Brown 1999; Grant 2001), with additional downdraft and momentum transport parameterizations.

The NCUM model is reconfigured to a regional domain (no nested) with different grid lengths of 12 km ($600 \times 600$ points; D1), 4 km ($1000 \times 1000$ points; D2), and 1.5 km ($400 \times 400$ points; D3) with 70 vertical hybrid levels (Fig. 1g; Jayakumar et al. 2017). In this study, three numerical experiments are carried out by considering different model horizontal resolutions, i.e., 12, 4, and 1.5 km, and the experiments are named NCUM12, NCUM4, and NCUM1.5, respectively. In all the numerical experiments, the model is integrated up to 72 h from 00 UTC of 26 July 2015. The boundary conditions for the experiments are provided by global NCUM forecast fields (Routray et al.
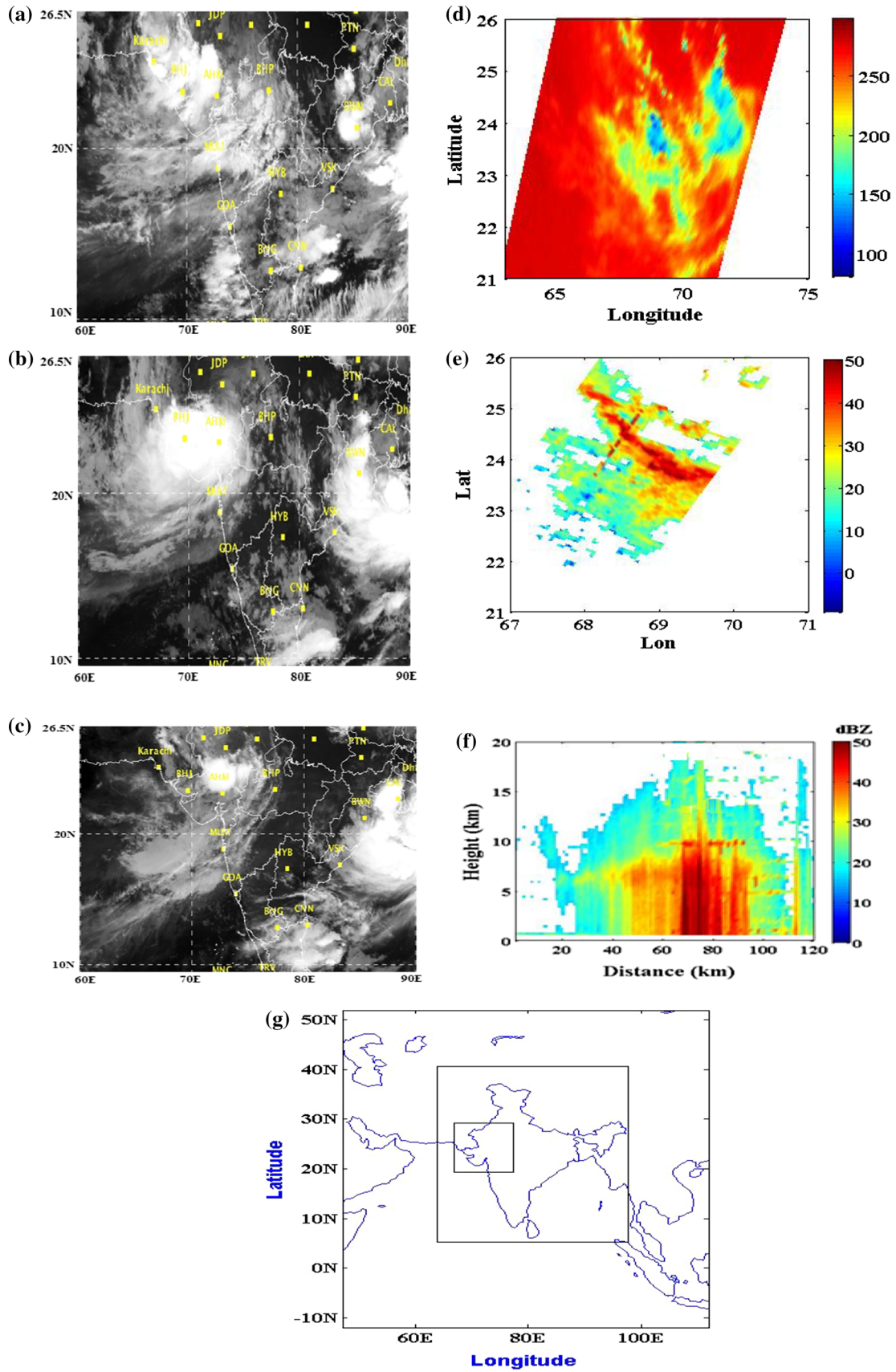
2017) interpolated onto the regional model co-ordinates. The initial conditions are provided to regional model from the NCUM global 4DVAR analysis system. The model integration time step is considered for NCUM12 (300 s), NCUM4 (60 s), and NCUM1.5 (60 s). The cumulus parameterization scheme, i.e., the mass flux convection with convectively available potential energy (CAPE) closure (Gregory and Rowntree 1990), is considered for NCUM12; however, the fully explicit treatment of convection for the NCUM4 and NCUM1.5 runs. The detail of the model configuration used in this study is given in Table 1.

Verification of the model outputs is an essential component of forecasting process. The model-simulated mean sea-level pressure (MSLP) and wind at different pressure levels are compared with the European Centre for Medium-Range Weather Forecasts Re-Analysis-Interim (ERA-I; resolution ~ 80 km). The meteorological fields of the low-resolution reanalyses have been interpolated into 12 km resolution through bilinear interpolation for comparison purposes.

The model simulations obtained from three numerical experiments are evaluated on the basis of calculation of direct position error (DPE) and absolute error (AE) for track and intensity of the MD, respectively. The DPE is the great-circle distance between the forecasted position of the MD and the observed position at the forecast verification time. The AE is magnitude of the difference between model forecast and observation.

An attempt is also made to verify the model-simulated rainfall through different skill scores using the NCMRWF-IMD Merged GPM Satellite-Rain-Gauge (NMSG) data of 0.5 degree resolution (Mitra et al. 2003, 2009). The model predicted rainfall is interpolated bilinearly to 50 km to match with the resolution of the observed data for verification purpose. In this purpose, different statistical skill scores viz. Heidke Skill Score (HSS), Hannssen–Kuiper skill score (HKS), and Critical Success Index (CSI) are calculated. These scores are considered to be among most useful ones for verification of severe weather forecasts (WMO report 2014).

The HSS is defined as follows:

$$HSS = \frac{2(ad - bc)}{[(a + c)(c + d) + (a + b)(b + d)]}$$

where *a*, *b*, *c,* and *d* are defined in the contingency (Table 2). The HSS is a skill score relative to random forecast. The range of the HSS is − 1 to 1. The negative value of HSS represents that the forecast skill is worse, i.e., random chance

forecast is better. The HSS value equal to 1 indicates a perfect forecast and 0 means no skill.

The mathematical expression of Critical Success Index (CSI) or Threat Score (TS) is

$$CSI = \frac{a}{(a + b + c)}.$$

The CSI ranges from 0 to 1, where 0 indicates no skill and 1 indicates perfect score. The score is sensitive to both the misses events and the false alarms.

Hannssen (1965) introduced a score known as Hannssen–Kuiper skill score (HKS) and also called true skill statistic. It is defined as

$$HKS = \frac{(ad - bc)}{(a + c)(b + d)}.$$

The HKS ranges from − 1 to 1, with 0 represents no skill and 1 indicates perfect score. The HKS is nothing but the difference between the hit rate and the false alarm rate. The skill score clearly suggests the occurrences and non-occurrences of the event. The HKS can be improved by increasing the hit rate without increasing the false alarm rate.

The rainfall is further verified with the object oriented method (entity-based or feature-based methods), i.e., Contiguous Rain Area (CRA) method (Ebert and McBride, 2000; Ebert and Gallus 2009). The CRA method is simply based on a pattern matching of two contiguous areas (entities), defined as the area of contiguous observed and forecast rainfall enclosed within a user-specified isohyets of precipitation. This feature-based method verifies the location, spatial pattern (size, shape), intensity, and other attributes of the feature. The total mean square error (MSE) can be decomposed into components due to location, volume and pattern error as given below:

$$MSE_{total} = MSE_{displacement} + MSE_{volume} + MSE_{pattern}$$

The total error due to displacement is equal to the difference between the mean square error before and after translation:

$$MSE_{displacement} = MSE_{total} - MSE_{shifted}.$$

The error component due to volume represents the bias in mean intensity:

$$MSE_{volume} = (F - X)^2,$$

where F and X are the CRA mean forecast and observed values after the shift. The pattern error accounts for differences in the fine structure of the forecast and observed fields:

$$MSE_{pattern} = MSE_{shifted} - MSE_{volume}$$

$$MSE_{shift} = \left(F' - X\right)^2,$$

where F' is the shifted forecast.

**(a)**



**(b)**



**(c)**
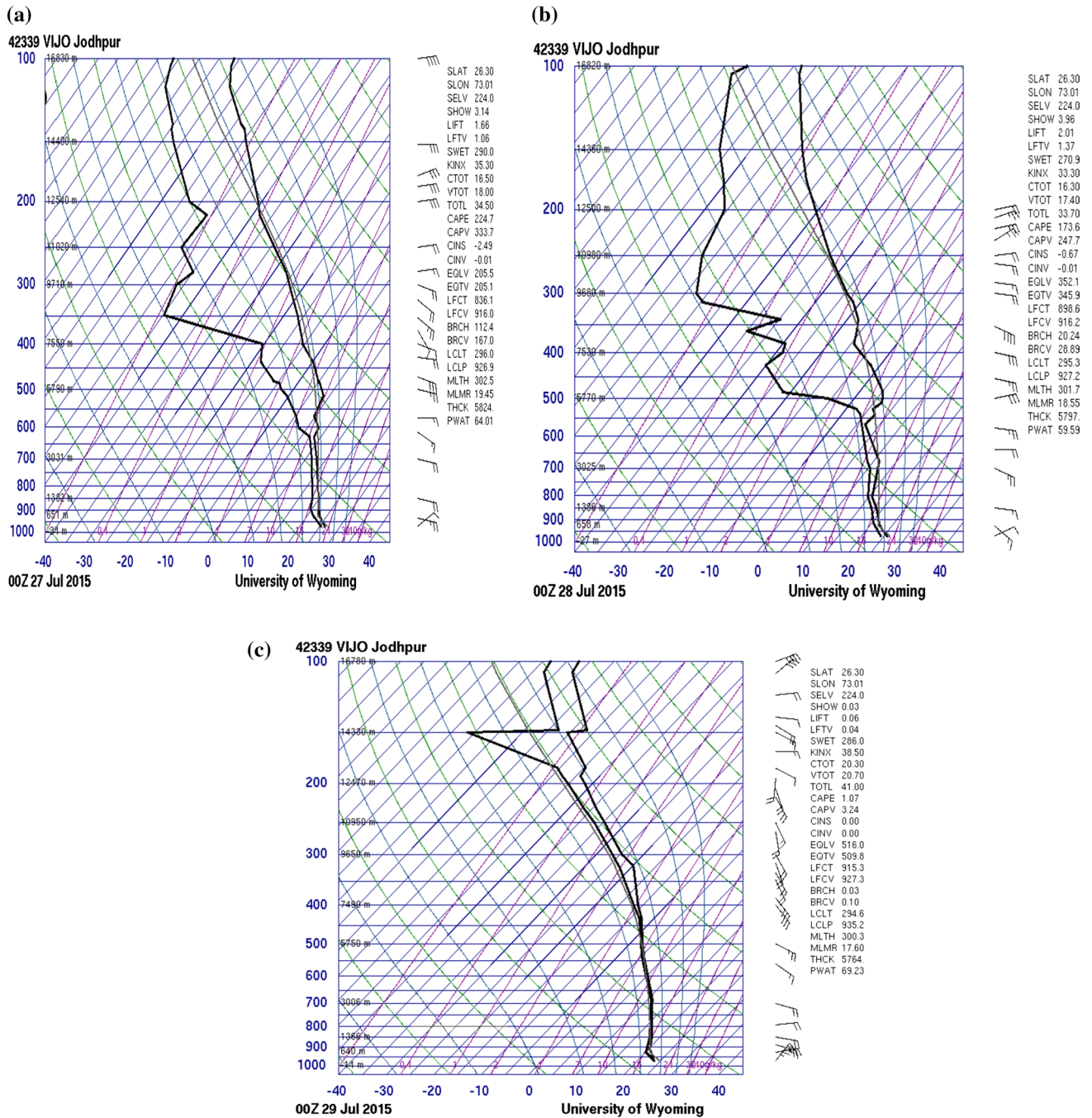


Fig. 2 Skew-T plot on **a** 27th **b** 28th and **c** 29th July 2015 at Jodhpur (26.3°N and 73.01°E). *source* http://weather.uwyo.edu/upperair/sounding.
html]

## 5 Results and discussion

The heavy rainfall occurred over many places of Gujarat and Rajasthan states during 27–29 July 2015 is simulated by the NCUM model to demonstrate and evaluate the skill of the model with different horizontal resolutions (12, 4, and 1.5 km). The impact of the model simulations with different resolutions is examined in the section, where the predicted meteorological fields during the acute/intense rainfall events are compared with the available observations from IMD rain-gauge station data and radiosonde/rawinsonde (RS/RW) (http://weather.uwyo.edu/upperair/sounding.html).

**Table 1** Overview of the regional NCUM model configuration used in the present study

| Parameters | 12 km | 4 and 1.5 km | |
|---|---|---|---|
| Governing equations | Complete equation (Non-hydrostatic); Deep atmosphere (Model top at ~ 80 km) | | |
| Horiz. resolution (N − S × E − W) | ~ 12 km (0.11*0.11) | ~ 4 km (0.36*0.36) | ~ 1.5 km (0.14*0.14) |
| | Pts. 600 × 600 | Pts. 1000 × 1000 | Pts. 400 × 400 |
| Vertical layers | L70 (terrain-following hybrid-height) | | |
| Model time step | 300 s | 60 s | |
| IC/data assimilation | Downscaling global analysis obtained from 4D-VAR analysis system | | |
| Spatial discretization | Finite difference method | | |
| Time Integration/advection | Semi-implicit Semi-Lagrangian scheme | | |
| Radiation process | Spectral band radiation with: (Zhong et al. 2008)<br>(i)Improved absorption of long-wave radiation by $CO_2$ and $O_3$<br>(ii) Improved use of climatological aerosol fields | | |
| Surface process | Joint UK Land Environment Simulator (JULES) land surface Scheme with (Smith et al. 2007)<br>(i)Use of TOPMODEL hydrology<br>(ii) Changes to the surface thermal and momentum roughness lengths | | |
| PBL process | First order non-local boundary layer scheme (Lock et al. 2000) with<br>(i) Reduced turbulent mixing for stably stratified boundary layers<br>(ii) Revised stability functions for unstable boundary layers<br>(iii)Revised diagnosis of shear-dominated boundary layers | | |
| Convection process | Mass flux convection Scheme(Gregory and Rowntree, 1990) with:<br>(i) increase of entrainment rate for deep convection<br>(ii) Smoothed adaptive detrainment of cloud liquid water, ice and tracers. | No | |
| Microphysics | Improved mixed-phase scheme based on Wilson and Ballard (1999) | | |
| Gravity wave drag | A new orographic drag scheme which contains better physical basis | | |
| Surface boundary condition | Surface Analysis + Climatology | | |

**Table 2** Contingency table used to compute the skill scores

| Events forecast | Event observed | |
|---|---|---|
| | Yes | No |
| Yes | a (Hits) | b (False alarm) |
| No | c (Miss) | d (Correct non-event) |

a: Event is predicted to occur (forecast occurrence) and it actually occurred

b: Event is predicted to occur but it does not observed in reality (observed non-occurrence)

c: Event is predicted not to occur (forecast non-occurrence), whereas it occurs in reality (observed occurrence)

d: Event is predicted not to occur (forecast non-occurrence) and it does not occur in reality (observed non-occurrence)

Total number of forecasts = a + b + c + d

### 5.1 Mean sea-level pressure (MSLP) and wind fields

The model simulated and ERA-I (verified analyses) of MSLP for day 1 and day 2 obtained from the three experiments are depicted in Fig. 3a–d, e–h, respectively. The simulated position of the MD in the NCUM1.5 experiment (Fig. 3d, h) is well matched with the ERA-I (Fig. 3a, e) in day 1 and day 2 simulations. These features are not seen in other simulations. The north-eastward movement of the MD is higher in the NCUM12 and NCUM4 as compared to the NCUM1.5 simulations. The intensity of the MD is well-simulated in the NCUM1.5 as compared to the NCUM12 and NCUM4 simulations. The MSLP from the ERA-I of the MD is 986 and 990 hPa in day 1 and day 2, respectively. The NCUM1.5 experiment (984 and 990 hPa) revealed the intensity of the MD relatively closer with the ERA-I as compared to the other simulations NCUM12 (990 and 986 hPa) and NCUM4 (989 and 985 hPa) in both days. It is also noticed that the intensity of the MD is also well-simulated in the NCUM4 experiment as compared to the NCUM12 experiment.

The model simulated and ERA-I winds at 850 hPa for day 1 and day 2 obtained from the three experiments are depicted in Fig. 3a–d, e–h, respectively. It is clearly seen from the figures that the magnitude of the wind speed is considerably higher (~ 5–10 m/s) surrounding the MD in the NCUM1.5 as compared to the other simulations as well as ERA-I. The well-structured MD is depicted in the NCUM1.5 simulations (Fig. 4d, h), which is not noticed in other simulations. The simulated position of the MD from NCUM1.5 is well matched with the ERA-I (Fig. 4a, e). However, the position of the MD simulated by NCUM12 and NCUM4 experiments shifted towards northeast from the position in the ERA-I analyses. The northeastward movement of the system is reasonably well-captured in the NCUM1.5 simulation as compared to the NCUM12 and NCUM4 simulations.
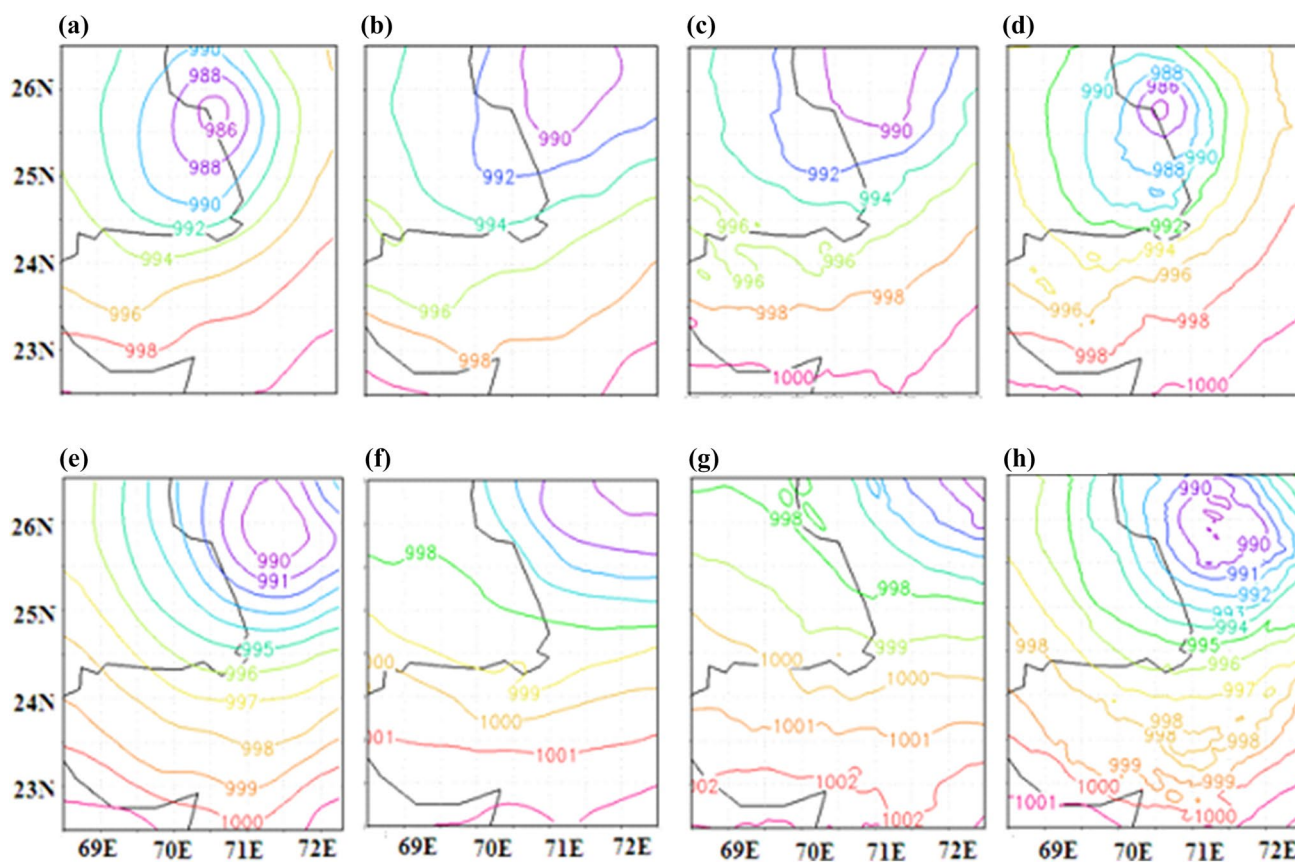
**Fig. 3** Mean sea-level pressure (MSLP; contour interval 2 hPa) from **a** ERA-I analysis, **b** NCUM12, **c** NCUM4 and **d** NCUM1.5 valid at 00 UTC 28th July 2015 (day 1). **e–h** are the same as (**a–d**) but for day 2 valid at 00 UTC 29th July 2015; contour interval 1 hPa

One important aspect of the intense MD is that the strong lower tropospheric westerlies winds at 900–850 hPa around 25–30 m/s are found surrounding the region (Krishnamurti et al. 1975; Daggupaty and Sikka 1977). This feature is well-reproduced by the NCUM1.5 simulation, which is not found in other simulations. Similarly, at the 500 hPa level, the NCUM1.5 (figure not provided) experiment simulated strong winds (~ 5–10 m/s) surrounding the MD, and these features are not represented well in the NCUM12 and NCUM4 simulations. The MD is clearly depicted in the NCUM1.5 simulations as compared to the other simulations. The features are reasonably well matched with the ERA-I.

The model-simulated magnitude of wind is further compared with the upper air observations (RS/RW) available over few stations, as provided in Table 3. In day 1, the strong magnitude of wind at 850 hPa is simulated by all the experiments as compared to the observations. However, the strong magnitude of the wind is simulated in the NCUM1.5 over Jodhpur station as compared to the other simulations. The magnitude of wind at 500 hPa is under-predicted by the model simulations; however, the magnitude of wind is reasonably improved in the NCUM1.5 simulation as compared to the others (Table 3). The error is reduced by around 2 m/s in NCUM1.5 over NCUM4 and NCUM12. Similarly, in day 2, the magnitude of wind at different pressure levels from NCUM1.5 simulation is well-matched with the observations. The improvement in the NCUM1.5 simulation is primarily due to the higher horizontal resolution, which properly represented the small-scale features associated with the large-scale monsoonal flow.

The skew-T plot at Jodhpur from three numerical experiments (NCUM12, NCUM4, and NCUM1.5) valid at 00 UTC 28 July 2015 (day 1) is depicted in Fig. 5a–c, respectively. The figure indicates that the whole atmosphere is unstable, whereas the maximum unstable is noticed at 300 hPa pressure level. This feature is well-correlated with the observed skew-T (Fig. 2b) plot over the region. It is worth to mention that the CAPE value is higher in the NCUM1.5 simulation (118 Jkg$^{-1}$) as compared to the NCUM12 (82 Jkg$^{-1}$) and NCUM4 (102 Jkg$^{-1}$) simulations. The CAPE value from NCUM1.5 simulation is closer with the observed value of CAPE (174 Jkg$^{-1}$), as shown in Fig. 2b. The CAPE value is improved by 68% in the NCUM1.5 simulation as compared to the
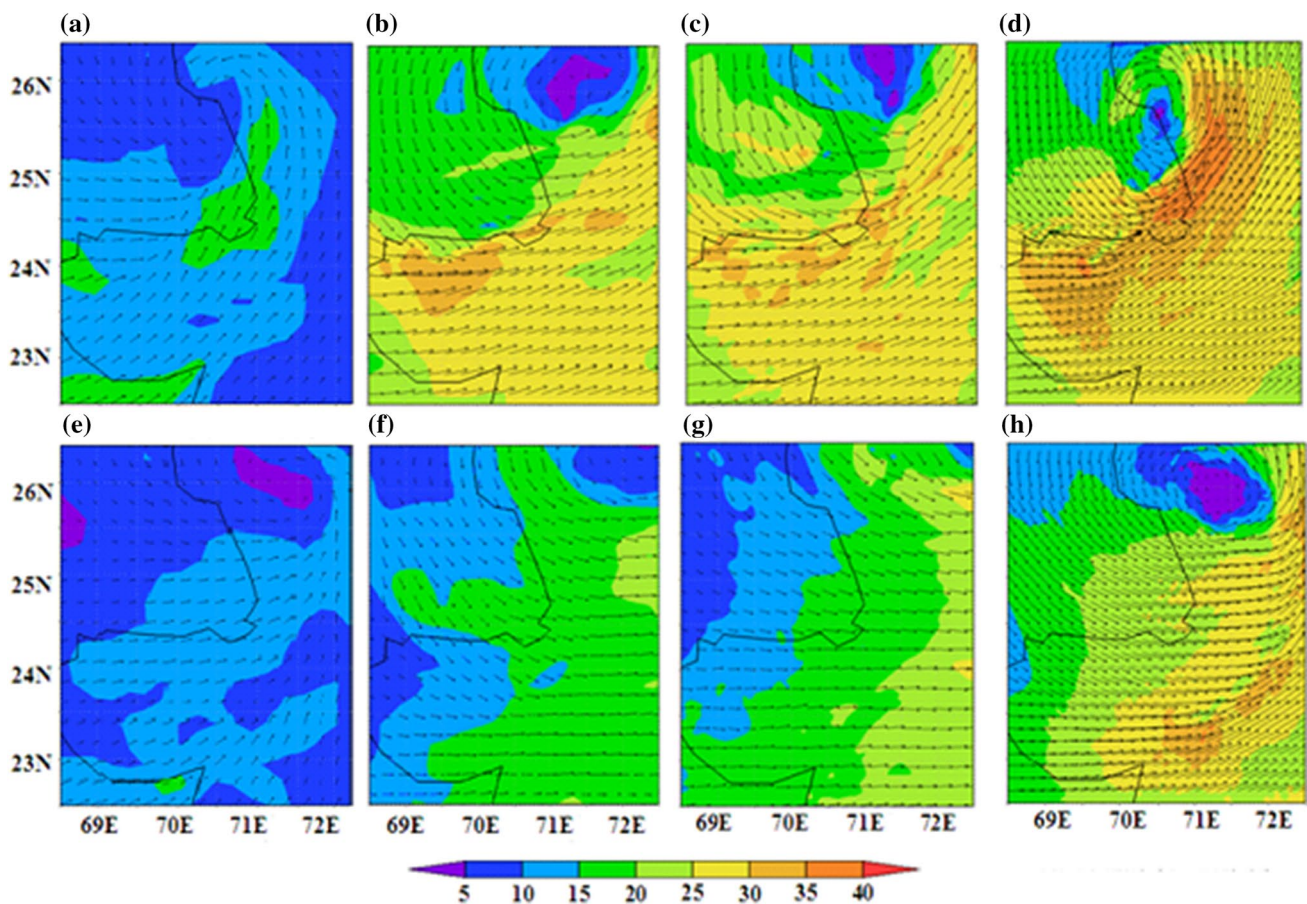
**Fig. 4** Same as Fig 3 but for wind vectors and magnitude (shaded; m/s) at 850 hPa

**Table 3** Observed and model-simulated winds (m/s) from three experiments at 850 and 500 hPa

| Name of Stations (lat. and lon.) | 28th July 2015 (day 1) | | | | | | | |
|---|---|---|---|---|---|---|---|---|
| | 850 hPa | | | | 500 hPa | | | |
| | OBS | NCUM12 | NCUM4 | NCUM1.5 | OBS | NCUM12 | NCUM4 | NCUM1.5 |
| Ahmadabad (23.06 and 72.63) | 20 | 24 | 24 | 23 | 12 | 6 | 6 | 9 |
| Jodhpur (26.3 and 73.01) | 15 | 21 | 23 | 24 | 16 | 8 | 9 | 11 |
| Mumbai (19.11 and 72.85) | 10 | 22 | 23 | 21 | NA | 11 | 15 | 17 |
| | 29th July 2015 (day 2) | | | | | | | |
| | 850 hPa | | | | 500 hPa | | | |
| Ahmadabad (23.06 and 72.63) | 26 | 19 | 22 | 26 | 13 | 8 | 13 | 13 |
| Jodhpur (26.3 and 73.01) | 22 | 11 | 16 | 22 | 13 | 16 | 8 | 10 |
| Mumbai (19.11 and 72.85) | 20 | 16 | 17 | 18 | NA | 3 | 7 | 11 |

*NA* Not Available

NCUM12 (47%) and NCUM4 (59%). During the day, the CIN remained very low in all the simulations. However, the CIN value is lower in the NCUM1.5 ($-0.03$ Jkg$^{-1}$) in comparison with the NCUM12 ($-0.13$ Jkg$^{-1}$) and

NCUM4 ($-0.33$ Jkg$^{-1}$) simulations. The observed CIN value is about $-0.67$ Jkg$^{-1}$. It is clear that the convective activity is more prominent in the NCUM1.5 simulation
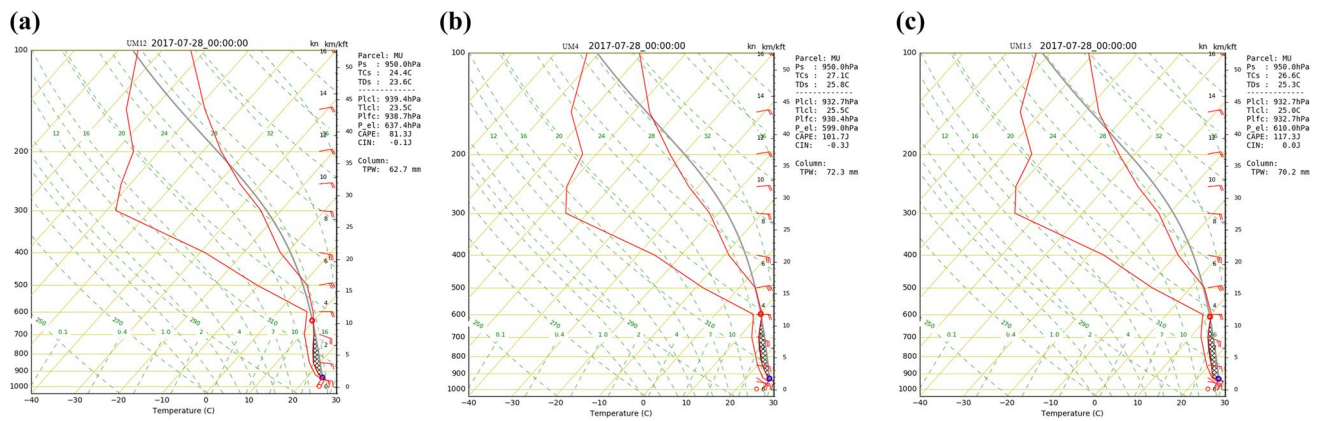
**Fig. 5** Skew-T plot at Jodhpur (Lat. 26.3°N and Lon. 73.01°E) from **a** NCUM12, **b** NCUM4, and **c** NCUM1.5 valid at 00 UTC 28th July 2015 (day 1)

than the other simulations. Hence, the intensity of the system is well-represented in the NCUM1.5.

## 5.2 Vorticity, moisture convergence, and moisture transport

The time–height cross section of vorticity ($10^{-5}$ s$^{-1}$) from NCUM12, NCUM4, and NCUM1.5 simulations during the period 00 UTC of 27–00 UTC 30 July 2015 to analyze the evolution of life span of the MD at different stages is shown in Fig. 6a–c, respectively. To keep in mind the intensity of the rainfall, the heavy rainfall period is divided into three stages such as developing stage (00 UTC 27th–00 UTC 28th July 2015), where the accumulated rainfall is less and the monsoon system intensified from low to depression stage; mature stage (00 UTC 28th–to 00 UTC 29th July 2015), where the rainfall intensity is high and intensity of the system vary from depression to deep depression stage; and finally, dissipating stage (00 UTC 29th–00 UTC 30th July 2015), while the rainfall is started decreasing and system became low pressure. The classification of the stages is done based on the synoptic conditions associated with the system during the period reported by IMD (report on Cyclones and depressions over the north Indian Ocean during 2015). It is clearly seen that the vertical structure of the MD is simulated reasonably well in all the experiments. However, the evolution and structure of the MD are more prominent in the NCUM1.5 simulation at different stages as compared to the other simulations. During the developing stage, the NCUM1.5 simulation (Fig. 6c) exhibits a structure of cyclonic vorticity ($15 - 20 \times 10^{-5}$ s$^{-1}$) at lower and upper levels which is not noticed in the NCUM12 (Fig. 6a) and NCUM4 (Fig. 6b) simulations. However, the positive vorticity ($5 - 15 \times 10^{-5}$ s$^{-1}$) is also noticed in the NCUM4 simulation which is very less in the NCUM12 simulation ($5 \times 10^{-5}$ s$^{-1}$). It is

noticed that the positive vorticity increased gradually from developing stage to mature stage and then started decreasing after 00 UTC 29 July 2015. The low-level divergent ($-5$ to $-9 \times 10^{-5}$ s$^{-1}$) extended up to 600 hPa is noticed during the dissipation stage (12 UTC 29 July 2015), and the features are not properly simulated by other simulations. The maximum positive vorticity ($15 - 25 \times 10^{-5}$ s$^{-1}$) is found during the mature stage and extended up to upper troposphere. It is evident that the gradual growth of the convective system which is well-represented in the NCUM1.5 simulation and leads to heavy rainfall events during the period. Similarly, the negative vorticity ($-9$ to $12 \times 10^{-5}$ s$^{-1}$) is seen at upper atmosphere around 200 hPa pressure level and above throughout this period.

Figure 6d–f shows the time–height cross section of moisture convergence ($10^{-4}$ g kg$^{-1}$ s$^{-1}$) from NCUM12, NCUM4, and NCUM1.5 simulations, respectively, during the period 00 UTC of 27 to 00 UTC 30 July 2015. It is seen that the convergence of moisture starts at lower atmosphere during developing stage in all simulations. The maximum value ($8 - 12 \times 10^{-4}$ g kg$^{-1}$ s$^{-1}$) of moisture convergence extended up to 600 hPa level is found in the NCUM1.5 simulation (Fig. 6f) during the mature stage. The horizontal extension of moisture convergence is more in the NCUM1.5 simulation than the other simulations. The feature is not well-simulated in the other experiments; however, the value of moisture convergence is improved in the NCUM4 (Fig. 6e) as compared to the NCUM12 (Fig. 6d) simulation. At the same time, the maximum divergence ($-12 \times 10^{-4}$ g kg$^{-1}$ s$^{-1}$) is found in the NCUM1.5 simulation at upper atmosphere is around 300 hPa. The low-level convergence and upper level divergence throughout this period are well-simulated by the NCUM1.5 experiment. In NCUM1.5 simulation, it is seen that the divergence ($-5 \times 10^{-4}$ g kg$^{-1}$ s$^{-1}$) developed around 700 hPa at 12 UTC 29 July 2015, which clearly evident that the system started dissipating. The intensity and depth of the
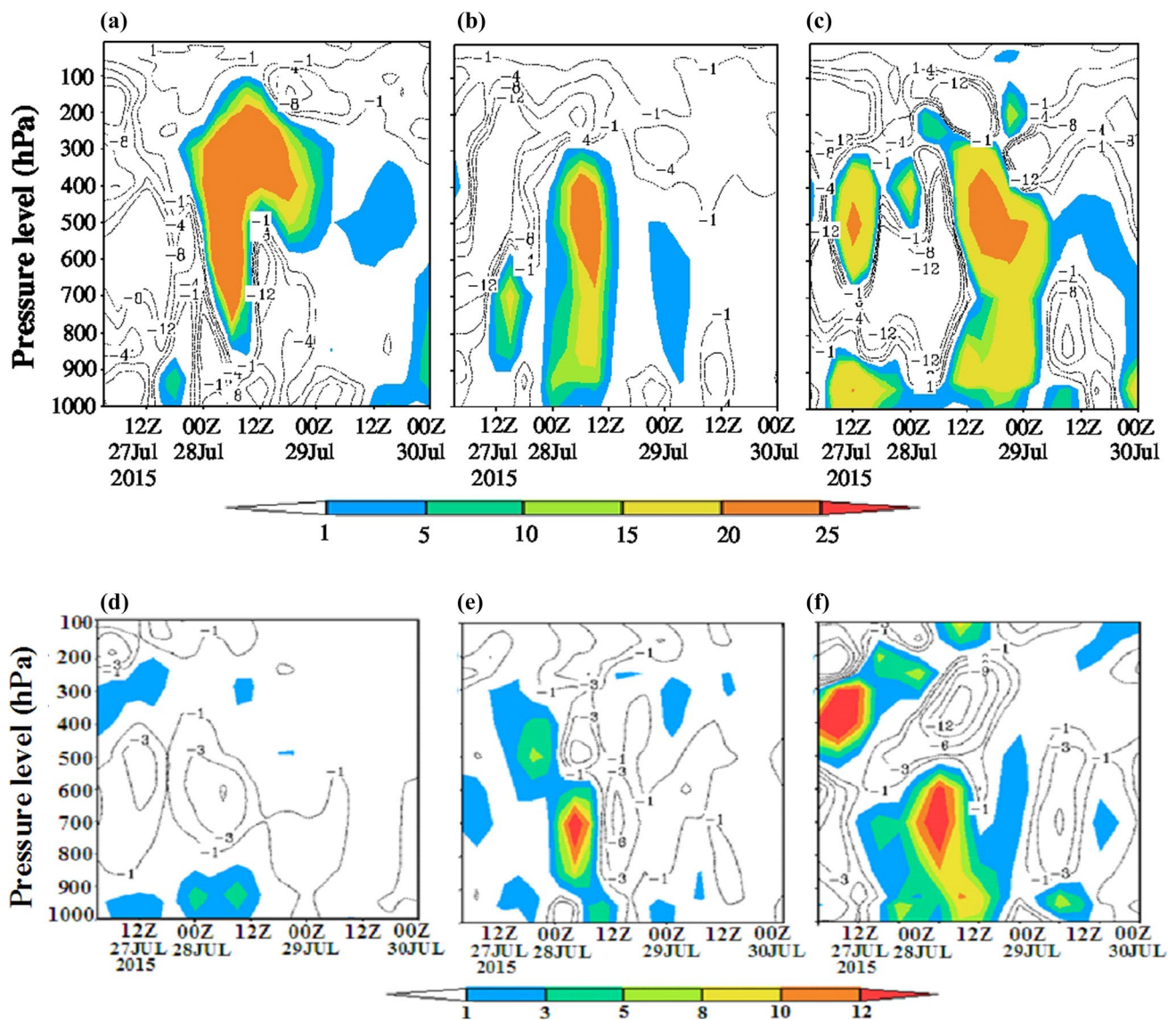
**Fig. 6** Time–pressure cross section of vorticity ($10^{-5}$ s$^{-1}$) at (25.0°N; 71.5°E) for **a** NCUM12; **b** NCUM4 and **c** NCUM1.5 valid at 00 UTC 27–30 July 2015. Similarly, **d–f** are the same as (**a–c**) but for moisture convergence ($10^{-4}$ g kg$^{-1}$ s$^{-1}$)

moisture convergence are gradually decreased as time progressed mainly from the mature stage to dissipating stages.

The moisture transport (vectors; kg.m$^{-1}$ s$^{-1}$) at 700 hPa and integrated precipitable water up to 300 hPa (shaded; mm) from ERA-I, NCUM12, NCUM4 and NCUM1.5 for day 1, as illustrated in Fig. 7a–d, respectively. It is noticed that the moisture transport is stronger in NCUM1.5 simulation (Fig. 7d) during the day as compared to the other simulations. The feature is comparable with the ERA-I analysis (Fig. 7a). However, the intensity simulated by the NCUM1.5 is slightly underestimated as compared to the ERA-I analysis. The moisture transport has a major impact on the mesoscale circulations (Stefanon et al. 2014), which leads to such a type of heavy rainfall event over the region.

The structure and position of the MD is well-captured in the NCUM1.5 simulation, which is resembled with the ERA-I analysis. Similarly, the integrated precipitable water for day 1 is found more by 5–10 mm and spreads over a large area in the NCUM1.5 simulation as compared to the other simulations. Particularly, for day 2 (figure not provided), the integrated precipitable water is not properly represented in NCUM12 and NCUM4 simulations. The simulations from NCUM1.5 of integrated precipitable water distribution show clearly the presence of organized convective activity leading to heavy precipitation.
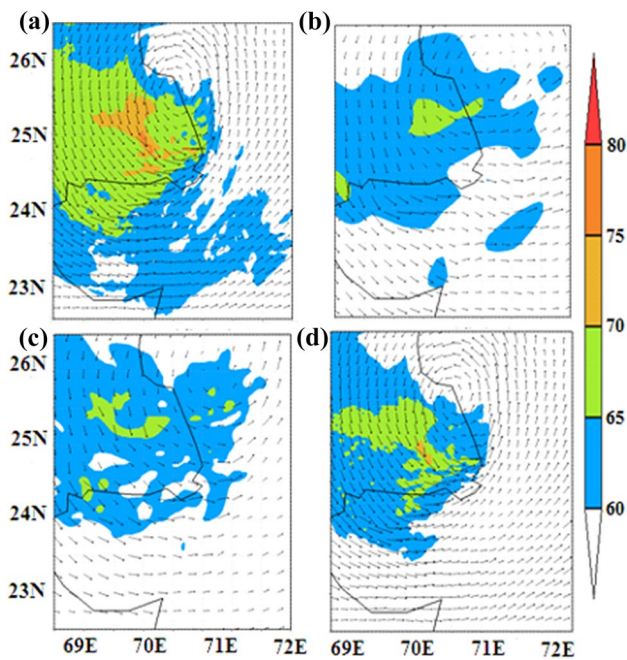
**Fig. 7** Moisture transport (vectors; kg/m/sec) at 700 hPa and integrated precipitable water up to 300 hPa (shaded; mm) from **a** ERA-I analysis, **b** NCUM12, **c** NCUM4 and **d** NCUM1.5 valid at 00 UTC 28th July 2015 (day 1)

## 5.3 Track and intensity errors

The Direct Position Error (DPE in km) in 12 h interval from all the numerical experiments along with the gain in skill (% of improvement) is depicted in Fig. 8a. It is noticed that the DPEs gradually increase with an increase of forecast length in all simulations. However, the DPEs at different forecast lead times are reasonably reduced in the NCUM1.5 simulation, which vary from 85 to 240 km as compared to NCUM4 (90–250 km) and NCUM12 (110–300 km) simulations. The mean DPEs are also less in the NCUM1.5 simulation (156 km) in comparison with the NCUM4 (167 km) and NCUM12 (198 km) simulations. However, the DPEs are also significantly reduced in the NCUM4 simulation than that of NCUM12 simulation. The NCUM1.5 simulation shows that the skill in track prediction of the MD is high with respect to NCUM4 and NCUM12 simulations. The mean DPEs from NCUM1.5 are substantially reduced by 7 and 22% in the NCUM1.5 simulation as compared to the NCUM4 and NCUM12 simulations, respectively. The mean DPEs from the NCUM4 simulation are also considerable reduced by 16% with respect to the NCUM12 simulation.

The absolute errors (AEs) along with skill (%, line) in intensity forecast based on 10 m maximum sustainable wind (MSW) for various forecast periods are shown in Fig. 8b. The evolution of intensity of the MD in different forecast

hours is reasonably well-simulated in the NCUM1.5 and NCUM4 simulations as compared to the NCUM12 simulation. The AEs of MSW are significantly reduced in the NCUM1.5 than the NCUM4 and NCUM12 simulations throughout the forecast lead times. The mean AEs of MSW are about 6, 8, and 10 kts in the simulation of NCUM1.5, NCUM4, and NCUM12, respectively. The skill varies from the range 9–15% (29–33%) in the NCUM1.5 simulation at different forecast hours with respect to the NCUM4 (NCUM12) simulation. The mean skill is high about 11 and 32% in the NCUM1.5 simulation with respect to NCUM4 and NCUM12 simulations, respectively. Similarly, the AEs of MSW are also less in the NCUM4 as compared to the NCUM12 simulation in all forecast hours. Therefore, the mean skill is high about 23% in the NCUM4 simulation compared to NCUM12 simulation. The percentage of error of AEs of MSW at different forecast hours is illustrated in Fig. 8c. It is noticed that the % of error of AEs is increased gradually with the increase of the forecast hours except at 12 h forecast. However, the errors are substantially reduced in the NCUM1.5 simulation throughout the forecast lead times as compared to the NCUM4 and NCUM12 simulations. Similarly, the errors are also considerably reduced in the NCUM4 than that of NCUM12 simulation. The mean of the % of error is about 39, 30, and 26% in the NCUM12, NCUM4, and NCUM1.5 simulations, respectively. From the result, it is clear that the track and intensity of the MD is properly resolved in the high resolution of the NCUM model.

## 5.4 Rainfall

The time series of area averaged (69–72°E and 23–25°N) 3 hourly accumulated model-simulated rainfall along with GPM satellite observation averaged over the experimental domain during the period 27–30 July 2015 depicted in Fig. 9. The observation shows two maximum rainfall spells at 9 and 24 h. However, the rapid increase of rainfall during 12–30 h may be due to the continuous restructuring of the meso-convective activities over the region which is influenced by the synoptic conditions. Subsequently, the rainfall intensity gradually decreased. The rainfall pattern is reasonably well-simulated by all the experiments. However, the intensity and pattern of the rainfall from NCUM1.5 is more close to the observation as compared to the other simulations. The two maximum rainfall spells are well-simulated in the NCUM1.5 experiment as compared to NCUM12 and NCUM4. However, the intensity and pattern of the rainfall are also improved in the NCUM4 simulation as compared with NCUM12 simulation. The root mean square error (RMSE) is less in the NCUM1.5 simulation (0.68 mm) as compared to the NCUM4 (1.22 mm) and NCUM12 (2.77 mm) simulations.

**Fig. 8** **a** Direct position errors (DPEs) of MD (left hand Y-axis) along with change in skill (line in right hand Y-axis, %); **b** Absolute Errors (AEs in left hand Y-axis, kts) of 10 m maximum sustainable wind (MSW) along with change in skill (line in right hand Y-axis, %) and **c** % of error of AEs



(a)

(b)

(c)
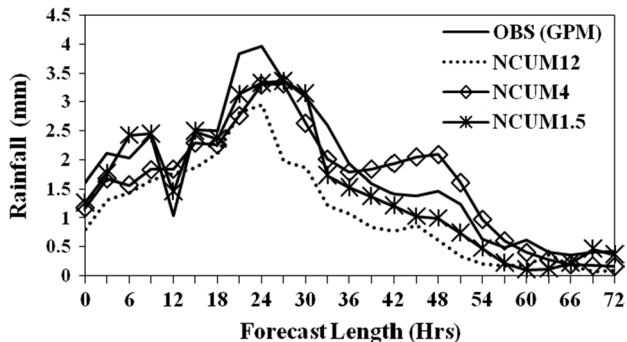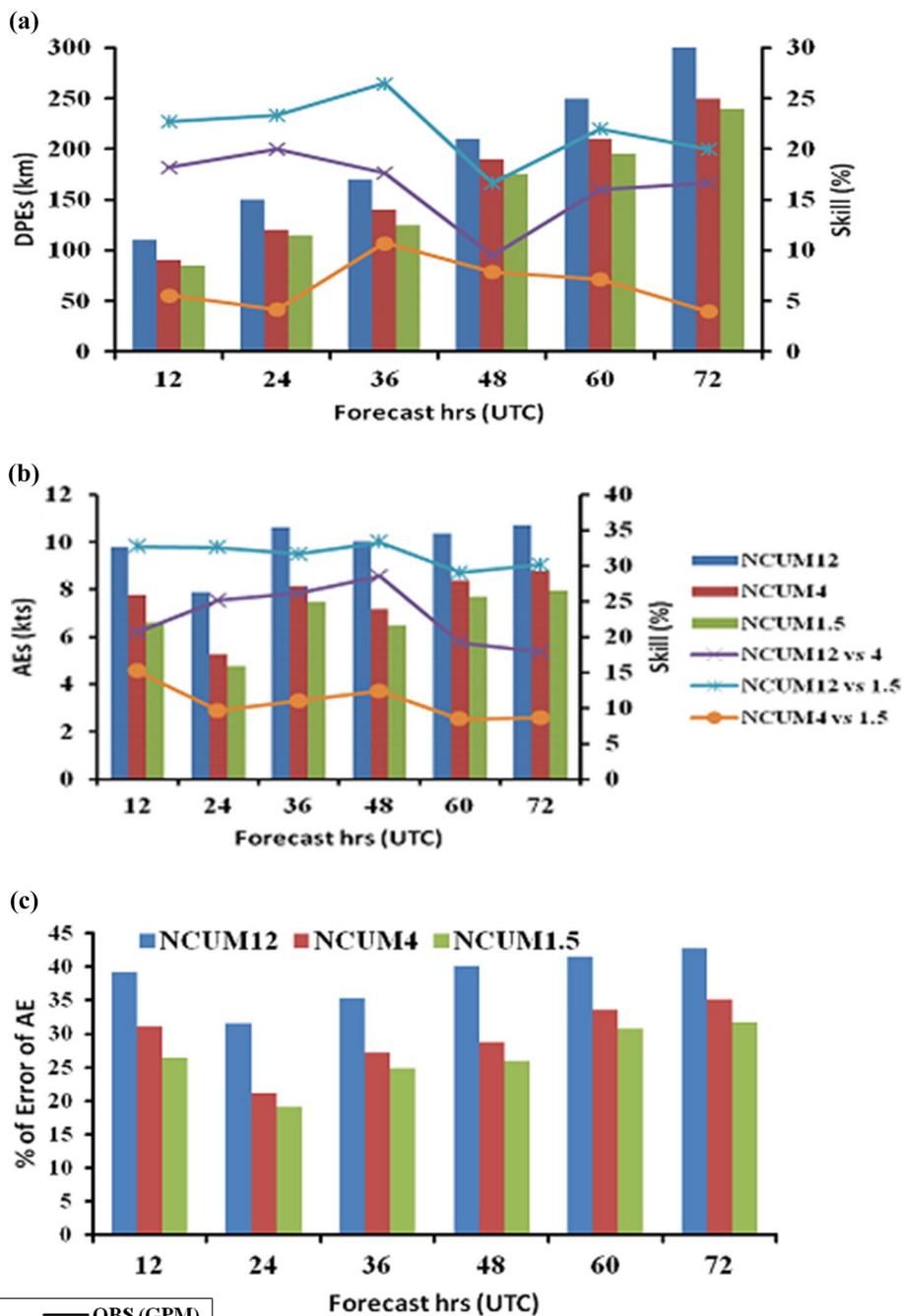


**Fig. 9** Time series of area averaged observed (GPM) and model-simulated 03 hourly rainfall (mm) from NCUM12, NCUM4 and NCUM1.5 valid at 00 UTC 27–30 July 2015 (23–25°N, 69–72°E)

The 24 h accumulated rainfall for day 1 and day 2 obtained from NCUM12, NCUM4, and NCUM1.5 simulations and the corresponding NMSG data (Mitra et al. 2003, 2009) are shown in Fig. 10. Comparisons of the 24 h accumulated model-simulated rainfall and station observed rainfall at the station location or nearest grid point is considered for day 1 and day 2 are given in Tables 4 and 5, respectively. In day 1, the observation (Fig. 10a) shows two patches of intense rainfall over the region. The features are simulated by all the simulations; however, the position of the intense rainfall is reasonably well-simulated in the
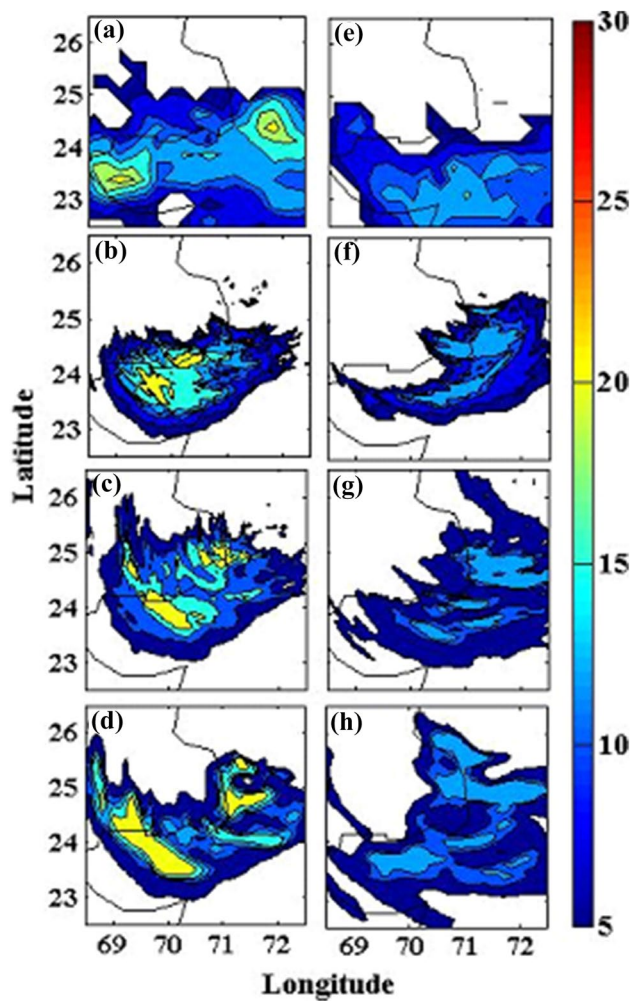
**Fig. 10** 24 h accumulated precipitations (cm) **a** NMSG; **b** NCUM12; **c** NCUM4 and **d** NCUM1.5 valid at 03 UTC 28 July 2015 (day 1). Similarly, **e**–**h** are the same as (**a**–**d**), respectively, but valid at 03 UTC 29 July 2015 (day 2)

NCUM1.5 experiment. The characteristic of the MD is that the heavy rainfall typically reaches 250 mm, mainly concentrated in the western and southwestern sectors of the depression (Sikka 1977). This feature is better simulated in the NCUM1.5 simulation (Fig. 10d) as compared to the other simulations. In day 1, the NCUM1.5 experiment simulated a well-organized closed circulation system. The features are also improved in the NCUM4 simulation as compared to the NCUM12 simulation.

During day 2, the spatial distribution of rainfall from model simulations is shifted towards northeast as compared to the observations (Fig. 10e). The scatter rainfall is seen over the region from both the simulations NCUM12 and NCUM4 (Fig. 10f, g). The NCUM1.5 simulation (Fig. 10h) shows well-organized convective bands of cloud around the system. Furthermore, compared with the model-simulated rainfall with the surface rain-gauge observations at specific stations, nearest grid points to the station locations are used. Both the surface and NMSG observation data indicate intense rainfall over the region. It is shown in Tables 4 and 5 that the amount of rainfall from NCUM1.5 simulation is reasonably well-matched with the observation as compared to the other simulations. During day 1, the locales of heavy precipitation (240 mm) recorded at the Sanchore station (24.75°N; 71.77°E) and the second maximum rainfall (190 mm) over Raniwada (24.75°N; 72.2°E) are well-captured in the NCUM1.5 experiment as compared to the NCUM12 and NCUM4 experiments (Table 4). However, the amount of intense rainfall is also significantly improved in the NCUM4 simulation as compared to the NCUM12 simulation.

IMD reported that the heavy precipitation (150–200 mm) occurred at five stations during day 2 (Table 5). The exact intensity of the rainfall is under-predicted by all the numerical experiments. However, the amount is simulated reasonably well in the NCUM1.5 as compared to NCUM4 and NCUM12 simulations. The average error is significantly reduced by 72% in the NCUM1.5 simulation, whereas

**Table 4** Comparison between stationwise observed and model-simulated rainfall (cm) for day 1 valid at 03 UTC of 28 July 2015

| Station Names | Lat. (deg) | Lon. (deg) | OBS | NCUM12 | NCUM4 | NCUM1.5 |
|---|---|---|---|---|---|---|
| Sanchore | 24.75°N | 71.77°E | 24 | 6 | 16 | 19 |
| Raniwada | 24.75°N | 72.20°E | 19 | 6 | 10 | 16 |
| Vadgam | 24.07°N | 72.49°E | 18 | 4 | 10 | 15 |
| Jalore | 25.120°N | 72.140°E | 18 | 4 | 5 | 16 |
| Bagoda | 25.21°N | 71.01°E | 18 | 5 | 10 | 12 |
| Jaswantpura | 24.80°N | 72.45°E | 16 | 5 | 8 | 12 |
| Amirgadh | 24.41°N | 72.64°E | 15 | 5 | 8 | 11 |
| Reodar | 24.61°N | 72.52°E | 12 | 5 | 7 | 9 |
| Sedwa | 25.74°N | 71.11°E | 9 | 5 | 6 | 8 |
| Gudamalini | 25.19°N | 71.71°E | 7 | 5 | 5 | 6 |
| Bhinmal | 25.01°N | 72.26°E | 7 | 3 | 5 | 6 |

**Table 5** Same as Table 4 but for day 2 valid at 03 UTC of 29 July 2015

| Station Names | Lat. (deg) | Lon. (deg) | OBS | NCUM12 | NCUM4 | NCUM1.5 |
|---|---|---|---|---|---|---|
| Radhanpur | 23.83°N | 71.61°E | 20 | 5 | 7 | 15 |
| Deodar | 23.98°N | 71.81°E | 17 | 4 | 8 | 10 |
| Harij | 23.69°N | 71.90°E | 15 | 6 | 6 | 12 |
| Sanchore | 24.75°N | 71.77°E | 15 | 6 | 10 | 10 |
| Visnagar | 23.70°N | 72.53°E | 11 | 2 | 6 | 8 |
| Pindwara | 24.79°N | 73.05°E | 7 | 2 | 3 | 6 |
| Erinpura | 25.14°N | 73.05°E | 7 | 2 | 4 | 5 |
| Sheoganj | 25.14°N | 73.06°E | 7 | 3 | 2 | 6 |
| Sumerpur | 25.15°N | 73.05°E | 7 | 3 | 3 | 5 |
| Pali | 25.77°N | 73.32°E | 7 | 2 | 3 | 5 |
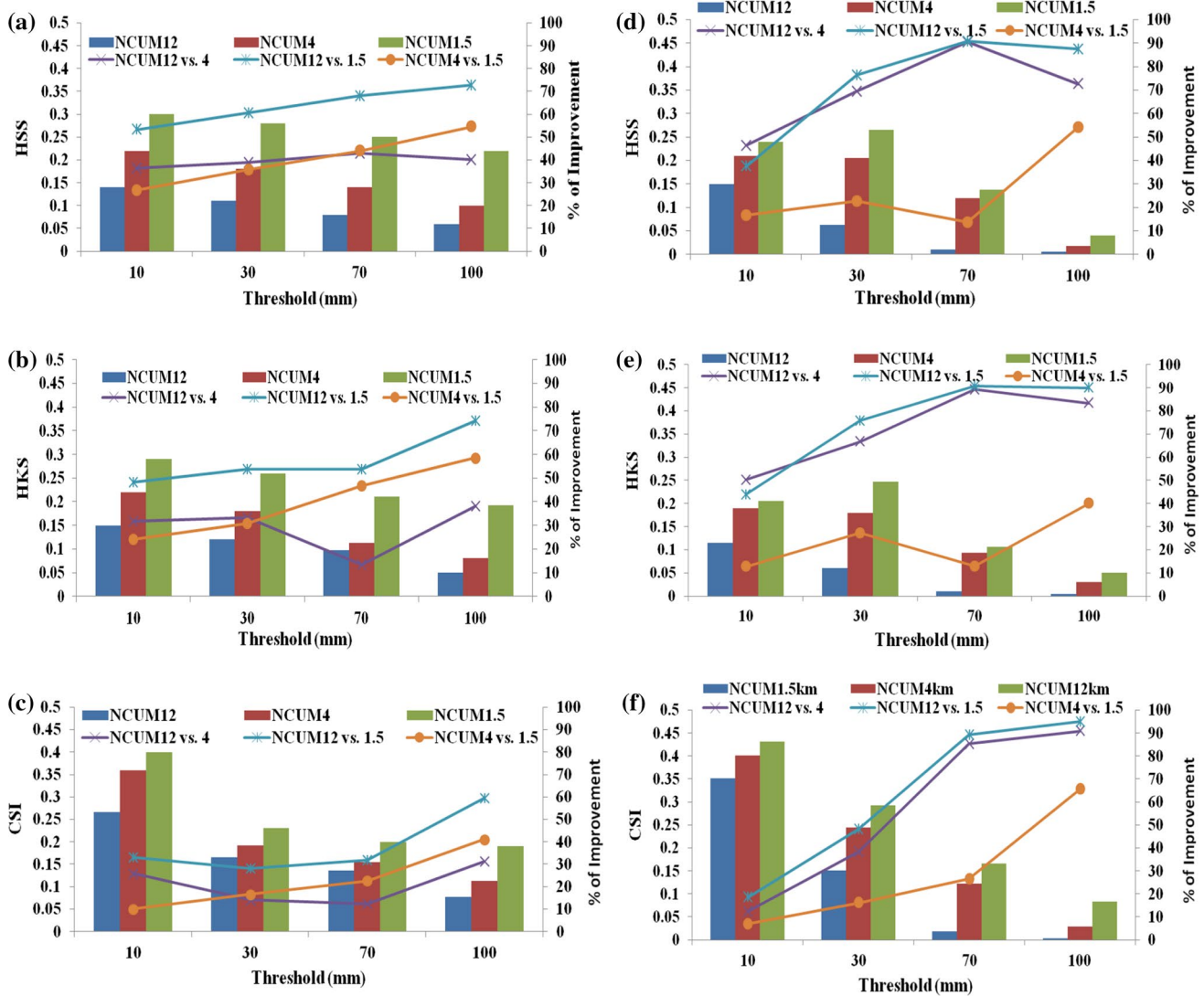


**Fig. 11** Statistical skill scores at different thresholds of rainfall (mm) **a** HSS; **b** HKS and **c** CSI along with % of improvement (line in right hand Y-axis) for day 1 valid at 00 UTC 28 July 2015. **d–f** are the same as (**a–c**) but for day 2 valid at 00 UTC 29 July 2015

the error is reduced by 46 and 36% in the NCUM4 and NCUM12 simulations, respectively. The increase of the resolution of NCUM model is capable to predict the high-intensity rainfall reasonably well. The forecast skill of the high-resolution NCUM model may be further improve by assimilating rain rate data through latent heat nudging, high dense and quality radar observations along other observations, etc. (Hawkness-Smith et al. 2012; Dixon et al. 2009).

The different statistical skill scores viz. HSS, HKS, and CSI of all experiments at different thresholds of rainfall (10, 30, 70, and 100 mm) are calculated for day 1 and day 2. The statistical skill scores along with percentage of improvement are depicted in Fig. 11a–c, d–f for day 1 and day 2, respectively. The HSS score gradually decreases with higher thresholds of rainfall in all simulations during days 1 and 2 (Fig. 11a, d). However, the HSS scores are higher in the NCUM1.5 simulation as compared to the NCUM4 and NCUM12 simulations. It is clearly seen that the HSS scores are quite less in NCUM12 simulation at higher thresholds (70 and 100 mm) during day 1 and day 2. The percentage of improvement is high in the NCUM1.5 with respect to the NCUM12 and NCUM4 simulations. Hence, the averaged skill of NCUM1.5 is about 67% (73%) and 40% (28%) over NCUM12 and NCUM4 simulations in day 1 (day 2), respectively. The skill of NCUM1.5 is significantly higher over the

NCUM12 than that of NCUM4. It is noticed that the HSS score is higher in the NCUM4 simulations as compared to the NCUM12 simulations during days 1 and 2. Hence, the averaged skill of NCUM4 is also high about 40 and 70% over NCUM12 in days 1 and 2, respectively.

The HKS score is illustrated in Fig. 11b, e. The HKS score is decreasing in the higher thresholds of rainfall in all simulations during days 1 and 2. It can be seen that the HKS score is appreciably improved in the NCUM1.5 as compared to the NCUM12 and NCUM4 simulations. However, the HKS score from NCUM12 is negligible at higher thresholds mainly in day 2. It is suggested that the NCUM12 is not able to properly resolve the convective activities over the region; hence, the high-intensity rainfall is under-predicted. The HKS score is also reasonably well-simulated by the NCUM4 as compared to the NCUM12 simulation. The % of improvement clearly depicted in the NCUM1.5 simulation at different thresholds with respect to other simulations. The averaged skill of NCUM1.5 is about 58% (75%) and 40% (23%) over NCUM12 and NCUM4 simulations in day 1 (day 2), respectively. Similarly, the CSI score (Fig. 11c, f) is reasonably well-simulated in the NCUM1.5 compared to NCUM4 and NCUM12. The % of skill is also considerably improved in the NCUM1.5 than that of NCUM4 and
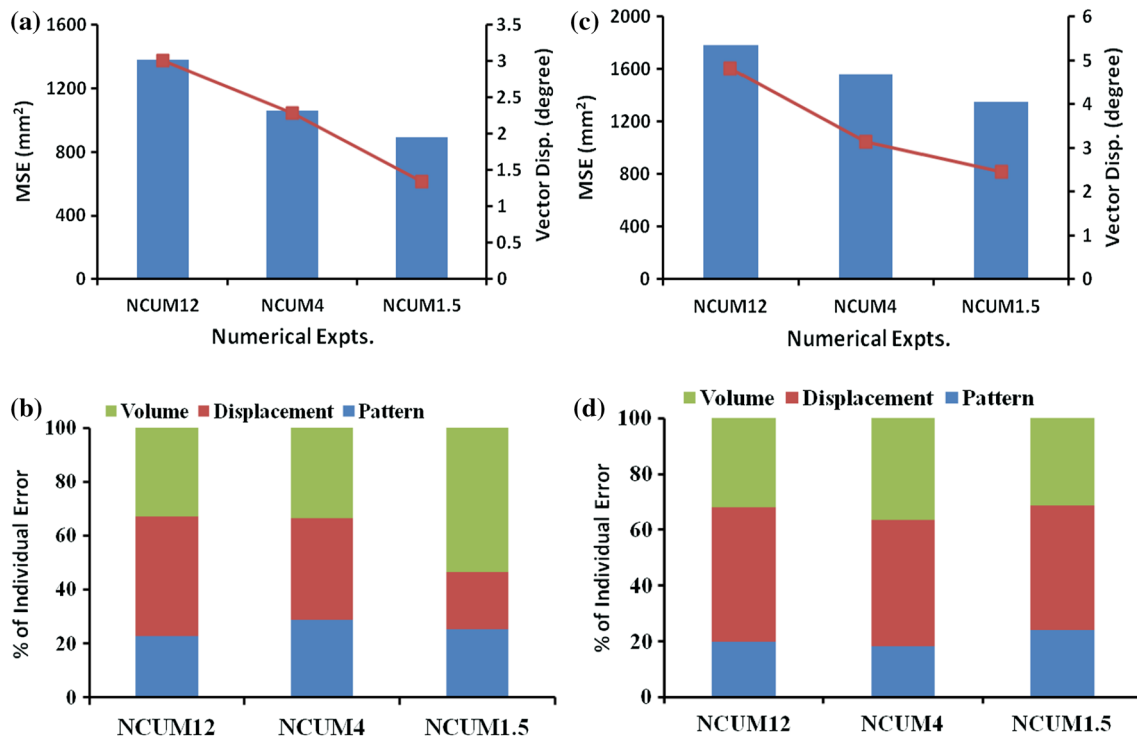


**Fig. 12** CRA verification of day 1 rainfall for threshold 5 cm **a** total Mean Square Error (MSE; bar in left hand *Y*-axis) along with vector displacement error (line in right hand *Y*-axis) **b** Percentage of contri-

bution of volume, displacement and pattern error. c, d are the same (**a**, **b**) but for threshold 10 cm

NCUM12. From Fig. 11, it is seen that skill score values at different thresholds are higher in day 1 than day 2.

The rainfall forecasts verification is further carried out using the CRA method based on pattern matching technique. The total mean square error (MSE) along with vector displacement error (line) and percentage of contribution from various components of MSE at different thresholds of rainfall (5 and 10 cm) for day 1 forecast are depicted in Fig. 12a–d. It is clearly seen that the MSE (Fig. 12a, c) is lesser in the NCUM1.5 simulation in both the thresholds as compared to NCUM4 and NCUM12 simulations. It implies that NCUM1.5 performs better than the other simulations in terms of matching the displacement, volume, and pattern of the forecast precipitation entities. The error is reduced by about 35% (24%) and 16% (14%) with the threshold 5 cm (10 cm) in the NCUM1.5 simulation with respect to NCUM12 and NCUM4, respectively. Similarly, the MSEs from both the thresholds are reasonably reduced in the NCUM4 than that of NCUM12. The gain in skill from the threshold 5 and 10 cm is higher in the NCUM4 about 23 and 12% than the NCUM12, respectively. The MSE from 10 cm threshold (Fig. 12c) is relatively high in all the simulations corresponding to the error from 5 cm threshold (Fig. 12a). Hence, the skill is less in all simulations as compared to the skill from 5 cm threshold.

The vector displacement error from the three simulations with threshold 5 and 10 cm is illustrated in Fig. 12a, d as plotted in line, respectively. The vector displacement error is determined using pattern matching. The forecast field is horizontally translated over the observed field until the best match is obtained. The vector displacement is then simply the location error of the forecast. From the figure, it is seen that the vector displacement error with both the thresholds is considerable reduced in the NCUM1.5 simulation as compared to the NCUM12 and NCUM4 simulations. It is evident that the location of the rainfall distribution is well-simulated by the NCUM1.5 than the other experiments. The error is reduced by about 56% (42%) and 49% (22%) in the NCUM1.5 for the threshold 5 and 10 cm with respect to the NCUM12 (NCUM4), respectively. Similarly, the location error is also reduced by 24 and 35% in the NCUM4 than the NCUM12 in both the thresholds.

The percentage of error from different components viz. location, volume, and pattern error which contributed to the total MSE at different thresholds is depicted in Fig. 12b, d. In NCUM1.5 simulation (Fig. 12b), it is clearly seen that the major error occurs due to the volume error of the rainfall in the forecast. However, the % of contribution due to the pattern and displacement error is comparatively less than the volume error. In other simulations (NCUM12 and NCUM4), the major error contributes to the total MSE due to the displacement error as compared to the volume and pattern errors. Correspondingly, the major error occurs due

to the displacement error of the rainfall in the forecast at the threshold 10 cm in all the simulations (Fig. 12d). However, the overall MSE at different thresholds is considerably less in the NCUM1.5 as compared to the other simulations (Fig. 12a, c).

# 6 Conclusion

The improvement of the forecast skill of heavy rainfall events associated with the monsoonal flow is an important aspect as they routinely result in flooding and significant loss of life and property over the Indian region. The study is carried to demonstrate and evaluate the skill of NCUM model with different horizontal resolutions (12, 4, and 1.5 km) in simulation of a heavy rainfall event (27–29 July 2015), which occurred over Gujarat and Rajasthan region (22°–25°N, 68.5°–78.5°E) due to the presence of MD during the active phase of the summer monsoon. For this purpose, three numerical experiments are carried out such as NCUM12, NCUM4 and NCUM1.5 by configuring the NCUM model with different horizontal resolutions 12, 4, and 1.5 km, respectively. The following conclusions are drawn from the study.

The CAPE value is improved by 47, 59, and 68%, in the NCUM12, NCUM4 and NCUM1.5, respectively. The CIN value is less in the NCUM1.5 as compared to the other simulations. A high CAPE and low CIN in NCUM1.5 causes the high-resolution simulation to capture the storm intensity well. The skew-T plot also suggested that the convection is more prominent in the NCUM1.5 simulation, which is reasonably well matched with the observation.

The position and northeastward movement of the MD is reasonably well represented in the high-resolution simulation (NCUM1.5) as compared to the NCUM12 and NCUM4 simulations. The features are well-correlated with the ERA-I analyses. The position errors of the MD are significantly reduced in the NCUM1.5 simulation. The strong lower tropospheric westerlies winds at 900–850 hPa are well represented in NCUM1.5 as one of the important aspects associated with the intense MD. The maximum positive vorticity is simulated by the NCUM1.5 during mature stage and extended up to upper troposphere as compared to the other simulations. It is clearly evident that the evolution and structure of the MD is more prominent in the high-resolution NCUM1.5 simulation at different stages than the other simulations.

The horizontal and vertical extension of moisture convergence is more prominent in the NCUM1.5 simulation than the other simulations at different stages of the MD. The analysis revealed that the NCUM12 simulation could not properly initiated the convection and the NCUM4 simulation somewhat initiate the convection for a small span.

However, the high-resolution NCUM1.5 simulation properly resolved convective activity and gives more realistic-looking features. Similarly, the moisture transport is also stronger in the NCUM1.5 simulation for day 1 and day 2 as compared to the other simulations.

The DPEs are gradually increased with an increase of forecast lead time in all simulations, while the errors are reduced in the NCUM1.5 simulation with different forecast hours as compared to other simulations. The positive impact on track prediction in the NCUM1.5 mainly attributed to the better interaction of storm environment with the surrounding large-scale flow due to the increase of resolution of the model. The mean DPEs are reduced by 7 and 22% in the NCUM1.5 with respect to NCUM4 and NCUM12 simulations. Similarly, the mean DPE from NCUM4 is also reduced by 16% over NCUM12.

The intensity forecast based on 10 m MSW is reasonably well-simulated in the NCUM1.5 as compared to other simulations. The mean skill from NCUM1.5 is high about 11 and 32% with respect to NCUM4 and NCUM12 simulations. Similarly, AEs from the NCUM4 simulation is improved by 23% than the NCUM12. More specifically, it has been demonstrated that the intensity of the MD is obtained due to the high resolution of NCUM simulations.

The mean percentage error of intensity is about 39, 30, and 26% in the NCUM12, NCUM4 and NCUM1.5 simulations, respectively, which suggested that the intensity of the MD is properly simulated in the high-resolution NCUM model.

The 3 hourly accumulated model-simulated rainfall pattern is reasonably well-simulated by all the experiments. However, the intensity and pattern of the rainfall from NCUM1.5 is more close to the observation as compared to the other simulations. The spatial distribution and locales of the heavy precipitation from NCUM1.5 simulation are reasonably well matched with the observation as compared to the other simulations. It is clearly seen that the various statistical skill scores at different thresholds are considerably improved in the NCUM1.5 simulations due to the increase of model horizontal resolution, which properly resolved the meso-convective features than that of other simulations.

It is clearly seen that the total MSE is lesser in the NCUM1.5 with the thresholds (5 and 10 cm) as compared to NCUM12 and NCUM4 simulations. The error in day 1 is reduced by about 35 and 16% with the threshold 5 cm in the NCUM1.5 simulation with respect to NCUM12 and NCUM4, respectively. Similar results also found for 10 cm threshold, where the MSE in NCUM1.5 simulation is reduced by 16 and 14% over NCUM12 and NCUM4 simulation, respectively.

The vector displacement error with both the thresholds (5 and 10 cm) is considerable reduced by about 56% (42%) and 49% (22%) in the NCUM1.5 simulation as compared to the NCUM12 (NCUM4) simulations, respectively. It is evident that the location of the rainfall distribution is well-simulated by the high-resolution NCUM1.5 than the other experiments.

This study demonstrated that running the NCUM model with higher horizontal resolution mainly 1.5 km improved the precipitation forecasts over the 12 km as well as 4 km. However, to further support this conclusion, case studies of diverse weather events and assimilation of radar observations along with other observations through advance data assimilation techniques like 4DVAR/Hybrid are required.

## References

Ashrit R, Sharma K, Dube A, Iyengar G, Mitra A, Rajagopal EN (2015) Verification of short-range forecasts of extreme rainfall during monsoon. Mausam 66(3):375–386

Benson L, Jr Charles, Rao VG (1987) Convective bands as structural components of an arabian sea convective cloud cluster. Mon Weather Rev 115:3013–3023

Bernardet LR, Grasso LD, Nachamkin JE, Finley CA, Cotton WR (2000) Simulating convective events using a high-resolution mesoscale model. J Geophys Res 105:14963–14982

Bhowmik SKR, Prasad K (2001) Some characteristics of limited-area model-precipitation forecast of Indian monsoon and evaluation of associated flow features. Meteorol Atmos Phys 76(3–4):223–236

Chang HI, Niyogi D, Kumar A, Kishtawal CM, Dudhia J, Chen F, Mohanty UC, Shepherd M (2009) Possible relation between land surface feedback and the post-landfall structure of monsoon depressions. Geophys Res Lett 36:L15826. https://doi.org/10.1029/2009GL037781

Charles AD (1993) Scientific approaches for very short-range forecasting of severe convective storms in the United States of America. In International Workshop on Observation/Forecasting of Mesoscale Weather and Technology of Reduction of Relevant Disasters Tokyo, Japan, 22–26 February 1993: 181–188

Chien FC, Mass CF, Neiman PJ (2001) An observational and numerical study of an intense land- falling front along the northwest coast of the US during COAST IOP2. Mon Weather Rev 129:934–955

Colle BA, Mass CF (2000) The 5–9 February 1996 flooding event over the Pacific Northwest: sensitivity studies and evaluation of the MM5 precipitation forecasts. Mon Wea Rev 128:593–617

Cullen MJP, Davies T, Mawson MH, James JA, Coulter SC, Malcolm A (1997) An overview of numerical methods for the next generation UK NWP and climate model. Atmos Ocean 35:425–444. https://doi.org/10.1080/07055900.1997.9687359

Daggupaty SM, Sikka DR (1977) On the vorticity budget and vertical velocity distribution associated with the life cycle of a Monsoon depression. J Atmos Sci 5:773–792

Das S, Ashrit R, Iyengar GR, Saji M, Das Gupta M, George JP, Rajagopal EN, Dutta SK (2008) Skills of different mesoscale models over Indian region during monsoon season: forecast errors. J Earth Syst Sci 117:603–620

Dash SK, Kulkarni MA, Mohanty UC, Prasad K (2009) Changes in the characteristics of rain events in India. J Geophys Res 114:D10109. https://doi.org/10.1029/2008JD010572

Davies T, Cullen MJP, Malcolm AJ, Mawson MH, Staniforth A, White AA, Wood N (2005) A new dynamical core for the Met Office's global and regional modeling of the atmosphere. Quart J Roy Meteor Soc 131:1759–1782

Davolio S, Mastrangelo D, Miglietta MM, Drofa O, Buzzi A, Malguzzi P (2009) High resolution simulations of a flash flood near Venice. Nat Hazards Earth Syst Sci 9:1671–1678. https://doi.org/10.5194/nhess-9-1671-2009

Deb SK, Kishtawal CM, Pal PK, Joshi PC (2008) Impact of TMI SST on the simulation of a heavy rainfall episode over Mumbai on 26 July 2005. Mon Wea Rev 136:3714–3741

Dixon M, Li Zhihong, Lean Humphrey, Roberts Nigel, Ballard Sue (2009) Impact of data assimilation on forecasting convection over the united kingdom using a high-resolution version of the met office unified model. Moth Wea Rev 137:1562–1584

Dube A, Ashrit R, Ashish A, Sharma K, Iyengar GR, Rajagopal EN, Basu S (2014) Forecasting the heavy rainfall during Himalayan flooding—June 2013. Weather Clim Extreme 4:22–34

Durai VR, Bhardwaj R (2014) Forecasting quantitative rainfall over India using multi-model ensemble technique. Meteorol Atmos Phys 126:31–48. https://doi.org/10.1007/s00703-014-0334-4

Ebert EE, Gallus WA (2009) Toward better understanding of the contiguous rain area (CRA) verification method for spatial verification. Weather Forecast 24:1401–1415

Ebert EE, McBride JL (2000) Verification of precipitation in weather systems: determination of systematic errors. J Hydrol 239:179–202

Essery R, Best M, Cox P (2001) MOSES 2.2 technical documentation. Met Office, Hadley Centre Tech. Note 30: 30 pp

Goswami BN, Venugopal V, Sengupta D, Madhusoodanan MS, Xavier PK (2006) Increasing trend of extreme rain events over India in a warming environment. Science 314:1442–1444

Grant ALM (2001) Cloud-base fluxes in the cumulus-capped boundary layer. Quart J Roy Meteor Soc 127:407–421

Grant ALM, Brown AR (1999) A similarity hypothesis for shallow-cumulus transports. Quart J Roy Meteor Soc 125:1913–1936

Gregory D, Rowntree PR (1990) A mass flux convection scheme with representation of cloud ensemble characteristics and stability-dependent closure. Mon Wea Rev 118:1483–1506

Hamada A, Takayabu YN (2016) Improvements in Detection of Light Precipitation with the Global Precipitation Measurement Dual-Frequency Precipitation Radar (GPM/DPR). J Atmos Ocean Tech 33:653–667. https://doi.org/10.1175/JTECH-D-15-0097.1

Hanssen AW, Kuipers WJA (1965) On the relationshipip between the frequency of rain and various meteorological parameters. Koninklijk Nederlands Meteorologisch Institut. Meded Verhand 81:2–15

Hawkness-Smith, Lee, Nicolas Gaussiat, Helen Buttery, Cristina Charlton-Perez, Sue Ballard, 2012: Variational assimilation of radar reflectivity data at the Met Office, ERAD 2012—The Seventh European Conference on Radar in Meteorology and Hydrology

Heikkilä U, Sandvik A, Sorteberg A (2011) Dynamical downscaling of ERA-40 in complex terrain using the WRF regional climate model. Climate Dyn 37:1551–1564. https://doi.org/10.1007/s00382-010-0928-6

Hong SY (2004) Comparison of heavy rainfall mechanism in Korea and the central US. J Meteor Soc Japan 82:1469–1479

Hou AY et al (2014) The global precipitation measurement (GPM) mission. Bull Amer Meteor Soc 95:701–722

Indian Meteorological Department (2016) Cyclones and depressions over the north Indian Ocean during 2015. Mausam 67(3):529–558

Jayakumar A, Sethunadh J, Rakhi R, Arulalan T, Mohandas S, Iyengar GR, Rajagopal EN (2017) Behavior of predicted convective clouds and precipitation in the high-resolution Unified Model over the Indian summer monsoon region. Earth Space Sci 4:303–313

Jung Joon-Hee (2016) Simulation of orographic effects with a Quasi-3-D multiscale modeling framework: basic algorithm and preliminary results. Jr Adv Model Earth Syst. https://doi.org/10.1002/2016MS000783

Kalnay E (2003) Atmospheric Modeling, Data Assimilation and Predictability. Cambridge University Press, Cambridge, p 364

Krishnamurti TN, Kanamitsu M, Godbole R, Chang CB, Carr F, Chow JH (1975) Study of a monsoon depression, Synoptic structure. J Meteor Soc Japan 53:227–240

Kumar A, Dudhia J, Rotunno R, Niyogi D, Mohanty UC (2008) Analysis of the 26 July 2005 heavy rain event over Mumbai, India using the weather research and forecasting (WRF) model. Quart J Roy Meteor Soc 134:1897–1910

Lean HW, Clark PA, Dixon M, Roberts NM, Fitch A, Forbes R, Halliwell C (2008) Characteristics of highresolution versions of the Met Office Unified Model for forecasting convection over the United Kingdom. Mon Wea Rev 136:3408–3424

Lee S, Lee D, Chang D (2011) Impact of horizontal resolution and cumulus parameterization scheme on the simulation of heavy rainfall events over the Korean Peninsula. Adv in Atmo Sci 28(1):1–15

Lock AP, Brown AR, Bush MR, Martin GM, Smith RNB (2000) A new boundary layer mixing scheme. Part I: scheme description and single-column model tests. Mon Wea Rev 128:3187–3199

Love David, Uhlenbrook Stefan, Corzo-Perez Gerald, Twomlow Steve, van der Zaag Pieter (2010) Rainfall–interception–evaporation–runoff relationships in a semi-arid catchment, northern Limpopo basin, Zimbabwe. Hydrol Sci J 55(5):687–703. https://doi.org/10.1080/02626667.2010.494010

Martin GM, Bush MR, Brown AR, Lock AP, Smith RNB (2000) A new boundary layer mixing scheme. Part II: tests in climate and mesoscale models. Mon Wea Rev 128:3200–3217

Mitra AK, Dasgupta M, Singh SV, Krishnamurti TN (2003) Daily rainfall for Indian monsoon region from merged satellite and rain-gauge values: large-scale analysis from real-time data. J Hydrometeorol (AMS) 4(5):769–781

Mitra AK, Bohra AK, Rajeevan MN, Krishnamurti TN (2009) Daily Indian precipitation analysis formed from a merge of rain-gauge data with the TRMM TMPA satellite-derived rainfall estimates. J Meteorol Soc Jpn 87A:265–279. https://doi.org/10.2151/jmsj.87A.265

Mohanty UC, Routray A, Krishna KO, Prasad K (2012) A Study on Simulation of Heavy Rainfall Events over Indian Region with ARW-3DVAR Modeling System. Pure Appl Geophys 169:381–399

Nielson-Gammon JW, Strack J (2000) Model resolution dependence of simulations of extreme rainfall rates. Preprints, Tenth PSU/NCAR Mesoscale Model Users Workshop, Boulder, pp 110–111

O'Hara JP, Webster S (2012) Assessing the sensitivity to horizontal resolution of Unified Model simulations of Hurricane Katrina. AGU Fall Meeting. https://doi.org/10.1029/2011MS000076

Orr A, Hosking JS, Hoffmann L, Keeble J, Dean SM, Roscoe HK, Abraham NL, Vosper S, Braesicke P (2014) Inclusion of mountain wave-induced cooling for the formation of PSCs over the Antarctic Peninsula in a chemistryclimate model. Atmos Chem Phys Discuss 14:18277–18314. https://doi.org/10.5194/acpd-14-18277-2014

Rajagopal EN, Iyengar GR, George JP, Gupta MD, Mohandas S, Siddharth R, Gupta A (2012) Implementation of Unified Model based Analysis-Forecast System at NCMRWF. NCMRWF technical report, NMRF/TR/2/2012

Rajeevan M, Kesarkar A, Thampi SB, Rao TN, Radhakrishna B, Rajasekhar M (2010) Sensitivity of WRF cloud microphysics to simulations of a severe thunderstorm event over Southeast India. Ann Geophys 28:603–619

Rama Rao YV, Hatwar HR, Salah AK, Sudhakar Y (2007) An experiment using the high resolution eta and WRF models to forecast heavy precipitation over India. Pure Appl Geophys 164:1593–1615

Routray A, Mohanty UC, Das AK, Sam NV (2005) Study of heavy rainfall event over the west-coast of India using analysis nudging in MM5 during ARMEX-I. Mausam 56:107–120

Routray A, Mohanty UC, Niyogi Dev (2010a) Simulation of heavy rainfall events over Indian monsoon region using WRF-3DVAR data assimilation system. Meteorol Atmos Phys 106:107–125

Routray A, Mohanty UC, Rizvi SRH, Niyogi D, Osuri KK, Pradhan D (2010b) Impact of Doppler weather radar data on simulation of Indian monsoon depressions. Quart J Roy Meteor Soc 136:1836–1850

Routray A, Mohanty UC, Krishna KO, Niyogi Dev (2016) Impact of satellite radiance data on simulations of Bay of Bengal tropical cyclones using the WRF-3DVAR modeling system. IEEE Trans Geosci Remote Sens 54:2285–2303

Routray A, Singh Vivek, Singh Harvir, Dutta Devajyoti, George John P, Rakhi R (2017) Evaluation of different versions of NCUM global model forsimulation of track and intensity of tropical cyclones over Bay of Bengal. Dyn Atmos Oceans 78:71–88

Sikka DR (1977) Some aspects of the life history, structure and movement of monsoon depressions. Pure Appl Geoph 115:1501–1529

Sikka DR, Gadgil S (1980) On the maximum cloud zone and ITCZ over the Indian longitudes during the southwest monsoon. Mon Wea Rev 108:1122–1135

Sikka DR, Rao PS (2008) The use and performance of mesoscale models over the Indian region for two high-impact events. Nat Hazards 44:35–372

Smith DM, Cusack S, Colman AW, Folland CK, Harris GR, Murphy JM (2007) Improved surface temperature prediction for the coming decade from a global climate model. Science 317:769–799

Stefanon M, Drobinski P, D'Andrea F, Lebeaupin-Brossier C, Bastin S (2014) Soil moisture–temperature feedbacks at meso-scale during summer heat waves over western Europe. Clim Dyn 42(5–6):1309–1324

Unnikrishnan CK, Gharai B, Mohandas Saji, Mamgain A, Rajagopal EN, Iyengar GR, Rao PVN (2016) Recent changes on land use/land cover over Indian region and its impact on the weather prediction using Unified model. Atmos Sci Let. https://doi.org/10.1002/asl.658

Vaidya SS, Kulkarni JR (2007) Simulation of heavy precipitation over Santacruz, Mumbai on 26 July 2005, using measascale model. Meteorol Atmos Phys 98:55–66

Wang W, Seaman NL (1997) A comparison study of convective parameterization schemes in a mesoscale model. Mon Wea Rev 125:252–278

Weisman ML, Skamarock WC (1997) The resolution dependence of explicitly modeled convective systems. Mon Wea Rev 125:527–548

Wilson DR, Ballard SP (1999) A microphysically based precipitation scheme for the UK Meteorological Office Unified Model. Quart J Roy Meteor Soc 125:1607–1636

World Meteorological Organization Report (2014), Forecast Verification in the African Severe Weather Forecasting Demonstration Projects, Published by Chairperson, Publications Board WMO, WMO-No. 1132, pages: 1–38

Xie B, Zhang F (2012) Impacts of typhoon track, island topography and monsoon flow on the heavy rainfalls in Taiwan associated with Morakot (2009). Mon Wea Rev 140:3379–3394

Zhang F, Sippel JA (2009) Effects of moist convection on hurricane predictability. J Atmos Sci 66:1944–1961

Zhong W, Osprey SM, Gray LJ, Haigh JD (2008) Influence of the prescribed solar spectrum on calculations of atmospheric temperature. Geophys Res Lett 35:L22813. https://doi.org/10.1029/2008GL035993

Zipser EJ, Cecil DJ, Liu C, Nesbitt SW, Yorty DP (2006) Where are the most intense thunder- storms on Earth? Bull Amer Meteorol Soc 87:1057–1071